Mussel Bed Boundaries as Dynamic Equilibria: Thresholds, Phase Shifts, and Alternative States

Megan J. Donahue,[1,2,*] Robert A. Desharnais,[1] Carlos D. Robles,[1] and Patricia Arriola[1,†]

1. Department of Biological Sciences, California State University at Los Angeles, Los Angeles, California 90032; 2. Hawaii Institute of Marine Biology, University of Hawaii, P.O. Box 1346, Kaneohe, Hawaii 96744

Submitted November 12, 2011; Accepted July 23, 2011; Electronically published October 5, 2011

Online enhancements: appendixes.

abstract: Ecological thresholds are manifested as a sudden shift in state of community composition. Recent reviews emphasize the distinction between thresholds due to phase shifts—a shift in the location of an equilibrium—and those due to alternative states—a switch between two equilibria. Here, we consider the boundary of intertidal mussel beds as an ecological threshold and demonstrate that both types of thresholds may exist simultaneously and in close proximity on the landscape. The discrete lower boundary of intertidal mussel beds was long considered a fixed spatial refuge from sea star predators; that is, the upper limit of sea star predation, determined by desiccation tolerance, fixed the lower boundary of the mussel bed. However, recent field experiments have revealed the operation of equilibrium processes that maintain the vertical position of these boundaries. Here, we cast analytical and simulation models in a landscape framework to show how the discrete lower boundary of the mussel bed is a dynamic predator-prey equilibrium, how the character of that boundary depends on its location in the landscape, and how boundary formation is robust to the scale of local interactions.

Keywords: threshold, boundary formation, stable states, hysteresis, size-dependent predation.

Introduction

Ecological thresholds are manifested as a sudden shift in state of community composition. Thresholds have received increasing attention across many ecological systems (Wilson and Nisbet 1997; Robles and Desharnais 2002; Pascual and Guichard 2005; Groffman et al. 2006; Mumby et al. 2009; Lauzon-Guay and Scheibling 2010; Osman et al. 2010) and may be characterized over space (e.g., a sudden shift in vegetation pattern along a continuous rainfall gradient; van de Koppel and Rietkerk 2004) or time (e.g., a rapid shift from coral to algal dominance in response to declining herbivore pressure; Mumby et al. 2009). Beginning with May (1977), theoretical approaches emphasized thresholds that result from multiple stable equilibria. In this case, two or more basins of attraction exist at a single point in parameter space (Petraitis and Dudgeon 2004), and initial conditions determine which equilibrium the system achieves. Multiple (or "alternative") stable states are of particular interest and concern for ecological systems exhibiting hysteresis: when a small parameter change results in a dramatic shift in system state that persists when the parameter change is reversed. This characteristic of ecological thresholds has garnered attention in conservation and ecosystem management because of the potential for rapid, irreversible ecological collapse in response to gradual environmental degradation (Muradian 2001; Scheffer et al. 2001; Huggett 2005).

Recent reviews (Dudgeon et al. 2010; Petraitis and Hoffman 2010) have emphasized the need to distinguish ecological thresholds that result from a switch between alternative stable states and those that result from phase shifts. Briefly (see Dudgeon et al. 2010 and Petraitis and Hoffman 2010 for a more detailed discussion), a phase shift is a shift in the location of a single equilibrium in state space in response to changes in environmental parameters; that is, the underlying environment changes, and, therefore, so does the community it can support. Phase shifts can be dramatic if changes in the environmental parameters are dramatic. In contrast, a switch between alternative stable states is a shift between two distinct equilibria in state space, both possible under the same environmental conditions, that can be difficult to reverse in the presence of hysteresis. For ecological thresholds that arise from multiple stable states, the underlying mechanism typically depends on positive feedback interactions along an environmental gradient in time or space. Mumby et al. (2009) models a coral-algal system where per capita mortality risk from grazing decreases as macroalgal density increases

* Corresponding author; e-mail: donahuem@hawaii.edu.
† Present address: Department of Mathematics, Los Angeles City College, Los Angeles, California 90029.

Am. Nat. 2011. Vol. 178, pp. 612–625.
0003-0147/2011/17805-52611$15.00.
DOI: 10.1086/662177

(positive feedback) and grazing pressure declines in time (temporal gradient in grazing). The model generates a switch from multiple equilibria to a single, stable, macroalgal-dominant equilibrium as grazing pressure declines. When multiple stable states give rise to thresholds in space rather than in time, the spatial scale of positive feedback must be local in order for densities to build up locally (van de Koppel et al. 2005). For example, van de Koppel and Rietkerk (2004) present a model of vegetation on an arid landscape where rainwater capture is enhanced by increased local vegetation density (positive feedback) on a spatial gradient of rainfall, resulting in a sharp break in the distribution of vegetation. Similarly, in a general model presented by Wilson and Nisbet (1997), abrupt thresholds in abundance arise when survivorship is enhanced by increased local density on a gradient of mortality.

Ecological thresholds arising from phase shifts and alternative stable states may also explain the characteristics of species' range limits (Holt et al. 2005). Typically, species' range limits are gradual, reflecting a decline in density with the continuous change of underlying niche axes (Holt et al. 2005), that is, a spatial phase-shift threshold. However, abrupt range limits can result from strong Allee effects: a negative per capita growth rate at low density creates an alternative stable equilibrium at zero density, which can result in an abrupt species boundary on a continuous gradient of habitat degradation (Holt et al. 2005), that is, a spatial alternative-stable-state threshold. In this study, we show (1) how continuous and abrupt species boundaries arise in the same underlying population model from phase shifts and alternative equilibria, respectively, (2) how these distinct threshold types can occur in close spatial proximity on real landscapes, (3) how the existence and location of the abrupt boundary depend on hysteresis, and (4) how the character of the boundary depends on the scale of local interactions.

Mussel beds have been a rich meeting ground for spatial theory and empiricism (e.g., Paine and Levin 1981; Wootton 2001; Robles and Desharnais 2002; Guichard et al. 2003; van de Koppel et al. 2005). While prior landscape models of mussel beds often focused on the dynamics and consequences of gap formation (Wootton 2001; Guichard et al. 2003), here we expand on the theory of boundary formation in mussel beds (Robles and Desharnais 2002; Donalson et al. 2004; Robles et al. 2010).

The original explanation of mussel bed limitation (Paine 1966, 1974; Connell 1972) maintained that the upper vertical boundary was set by physical stress (desiccation and high temperature) while the lower boundary was set by intense predation by the sea star *Pisaster ochraceus*. How predation determined the lower boundary was of particular interest because the boundary remains stationary despite high interannual variation in mussel recruitment. The shore level of the lower boundary was believed to be fixed by the intolerance of *Pisaster* to exposure at low tide. Thus, the upper shore provided a spatial refuge for the desiccation-resistant *Mytilus californianus* from desiccation-susceptible *Pisaster*. Recent work proposed (Robles and Desharnais 2002) and experimentally demonstrated (Robles et al. 2009, 2010) that the lower boundary is a dynamic equilibrium along continuous gradients of prey production and predator attack rate. The dynamic-equilibrium concept is more consistent with observational and experimental data than is an inviolable refuge: *Pisaster* are often observed foraging above the lower mussel bed boundary (Robles et al. 1995), and recent experiments (Robles et al. 2009) demonstrate both the downward extension of the lower boundary when *Pisaster* are removed (confirmation of Paine's 1974 result) and the upward retraction of the lower boundary when *Pisaster* are added (contra the fixed-refuge hypothesis). It is this dynamic model of mussel bed boundary formation that we investigate here.

To understand the dynamic properties of the *Mytilus-Pisaster* model, we pair nonspatial ordinary differential equations (ODE model) with a spatially explicit, stochastic cellular automaton (CA model; Wilson and Nisbet 1997), which simulates mussel bed structure on an idealized intertidal landscape. The ODE model is a mean-field approximation of the CA model and gives insight into the equilibrium dynamics of the system for the full range of parameter values. When run on a homogeneous landscape, the CA model is a stochastic simulator of the ODE model, but the flexibility of the CA model opens our investigation to the effects of local interactions and heterogeneous landscapes on dynamics and pattern formation.

ODE Model

We consider here the dynamics of a single mussel bed and, therefore, model *Mytilus-Pisaster* interactions as an open system (fig. 1). At any location in the mussel bed, the supply of *Mytilus* recruits is constant, and recruitment rate depends on available space. A newly settled mussel grows

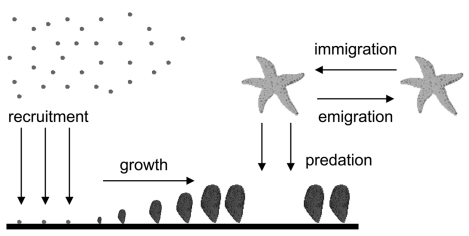

Figure 1: Schematic of model processes illustrating open recruitment, growth, and predation of mussels and immigration and emigration of sea stars.

Table 1: Parameter definitions and default values for mean-field model

Symbol (units)	Default value	Description
s_0 (mm)	1.0	Size at recruitment
σ (cell^{-1} day^{-1})	1.0 (.001–1.25)	Recruitment rate
k (cell^{-1})	1.0	Saturation density of mussels
β (day^{-1})	.0007	Decrease in mussel growth rate with size
s_∞ (mm)	200 (30–200)	Asymptotic size of a mussel
$s\mu_0$ (day^{-1})	.0001	Background per capita mussel mortality rate
θ (cells day^{-1})	1.0 (0–1)	Per capita predator attack rate
c (cells mm^{-1})	.04	Decrease in predator attack rate with mean mussel size
I (cell^{-1} day^{-1})	.01	Per capita predator immigration rate
e_0 (mm day^{-2})	5.0	Per capita predator emigration constant per unit prey consumed

Note: For the three parameters (σ, θ, and s_∞) that vary in the two-dimensional gradient model, the maximum and minimum values are listed in parentheses.

asymptotically to a maximum size and, in the process, becomes increasingly resistant to predation (Paine 1976); small mussels also become more resistant to predation when surrounded by larger mussels (Bertness and Grosholtz 1985; Fong 2009). Sea stars immigrate into the system at a constant rate, but their emigration rate depends on the availability of mussel prey, an expression of the predator's aggregative response to changing prey abundance (Robles et al. 1995). The ODE model assumes that the environment is homogeneous, that is, that there are no environmental gradients or local interactions affecting recruitment, growth, or predation. In the ODE model, we examine environmental heterogeneity by varying the model parameters that determine settlement, growth, and predator attack rate, which depend on the location in the landscape. For example, at low tidal heights, mussels spend more time submerged and therefore experience higher growth rates and higher predation risk; in areas with direct wave exposure, more water flow leads to higher recruitment, higher growth rates, and lower predation risk.

Our derivation of the mean-field ODE model (see app. A, available online) begins with the McKendrick–von Foerster equation for an age-structured population and the von Bertalanffy function for individual growth. Following Nisbet et al. (1997), we introduce variables $S(t)$ for the mean size density of mussels (mean mussel size per unit area, including empty cells of size 0) and $N(t)$ for mean numerical density of mussels (number of mussels per unit area). Since the unit area is equal to one cell in the CA model, $N(t)$ is equivalent to the proportion of space occupied by mussels, and $S(t)$ can be thought of as the average size of mussels when the average size includes empty cells of size 0. Local spatial effects in the CA model are replaced by these mean-field global values. The result is a system of three ordinary differential equations (derived in app. A) describing the dynamics of mean mussel size density, mean mussel numerical density, and predator density in a well-mixed, spatially homogeneous patch (i.e., uniform tidal height and wave exposure):

$$\frac{dS(t)}{dt} = s_0\sigma(1 - N(t)k^{-1}) + \beta(s_\infty N(t) - S(t)) - (\mu_0 + \theta P(t)e^{-cS(t)})S(t), \quad (1a)$$

$$\frac{dN(t)}{dt} = \sigma(1 - N(t)k^{-1}) - (\mu_0 + \theta P(t)e^{-cS(t)})N(t), \quad (1b)$$

$$\frac{dP(t)}{dt} = I - e_0 P(t)(\theta S(t)e^{-cS(t)})^{-1}. \quad (1c)$$

Equations (1a) and (1b) describe, respectively, the change in mean size density and mean numerical density through time. Mean size density (eq. [1a]) changes through (1) recruitment of size-s_0 mussels into unoccupied space at maximum recruitment rate σ, which declines to 0 as the mussel bed approaches its saturation density $k = 1$ mussel cell^{-1}; (2) von Bertalanffy growth of all mussels at maximum growth rate β, which declines as $S(t)$ approaches its maximum value $s_\infty N(t)$, the maximum individual size times the proportion of occupied space; and (3) size-independent background mortality at rate μ_0 and size-dependent predator-induced mortality at maximum rate θ, which declines with increasing mean size density at an exponential rate c. Mean mussel numerical density (eq. [1b]) (1) increases with mussel recruitment at a maximum recruitment rate σ, which declines as the mussel bed approaches its saturation density k, and (2) decreases with background mortality at rate μ_0 and with predator-induced mortality at a maximum rate θ, which declines exponentially with increasing mussel size density. Predators (eq. [1c]) immigrate into the system at a constant rate I and emigrate at a rate inversely proportional to the per capita rate at which predators consume prey. Model parameters are listed in table 1.

Setting the time derivatives of equation (1) to 0 gives the joint predator-prey equilibrium (S^*, N^*, P^*). As shown in appendix A, the equilibrium mean mussel size density S^* is given by the roots of the following function:

$$f(S) = s_0\sigma + \frac{\sigma(s_\infty\beta - s_0\sigma k^{-1})}{\sigma k^{-1} + \mu_0 + (I\theta^2/e_0)Se^{-2cS}} - \left[\beta + \mu_0 + \left(\frac{I\theta^2}{e_0}\right)Se^{-2cS}\right]S. \quad (2)$$

Once the equilibrium value S^* has been obtained, the remaining equilibrium values are given by

$$P^* = \left(\frac{I\theta e^{-cS^*}}{e_0}\right)S^*, \quad N^* = \frac{\sigma}{\sigma k^{-1} + \mu_0 + (I\theta/e_0)S^*e^{-2cS^*}}. \quad (3)$$

Spatial Model: Structure and Assumptions

Representation of Space

The spatially explicit cellular-automaton (CA) model is a stochastic simulator of the ODE model to which environmental gradients and spatially local interactions can be added. In the CA model, the intertidal landscape is represented as a rectangular lattice of cells, where each cell is a potential site for a mussel. Each cell is identified by its (x, y) coordinate in a $w \times h$ lattice, where the horizontal dimension represents alongshore position and the vertical dimension represents tidal height; x and y coordinates are scaled to vary from 0 to 1. In this study, all simulations are run on lattices of 2,000 × 2,000 cells. Each cell can take on integer state values representing mussel size. The state of a cell in position (x, y) at time t is $S_{xy} \in \{0, 1, \ldots, s_{\infty,xy}\}$, where 0 is an empty cell, 1 is a cell with a newly recruited mussel, and $s_{\infty,xy}$ is the asymptotic maximum size of a mussel at a particular (x, y) coordinate. Model dynamics are described as stochastic transitions between states, where the transition probabilities for any given cell are determined by the current state of the cell (size effects), the states of the surrounding cells (neighborhood effects), and the cell's position in the lattice (gradient effects). Gradient effects represent tidal exposure in the y-dimension and wave energy in the x-dimension, such that a cell's position along these gradients determines physical stress and the flux of recruits and food particles to the rock surface. The transition probabilities therefore represent position-specific mussel recruitment, growth to larger sizes, and predator-induced mortality. While there are numerous empirical studies indicating the direction of change of the parameters over the gradients described below, specific functional forms are usually not known. In the following description of parameterization, we chose the simplest functional form indicated by existing data. Default parameter values (table 1) were derived from the literature and unpublished studies, as described below.

Mussel Recruitment

Spatial patterns of mussel recruitment are, perhaps, the least understood aspect of mussel ecology. *Mytilus californianus* recruitment probabilities often increase with wave energy along a given shore level (Menge 1992; Robles 1997; Moya 2005). Plankton collections taken just offshore (<20 m) from mussel beds revealed competent larvae concentrated in the top 2 m of the water column (C. D. Robles, unpublished data). Given shore level variation in tidal emersion and greater vertical mixing of wave-exposed shores (Denny 1988; Denny and Shibata 1989), this observation predicts a vertical profile of settlement with a midshore peak and a wider vertical spread on wave-exposed shores. This prediction was confirmed by empirical measurements of mussel recruitment along tidal-height and wave-energy gradients that revealed a peak occurring in the mid-intertidal zone at the wave-exposed extreme and decreasing toward lower wave energies and more extreme shore levels (Robles 1997; see app. B, available online). When the CA model includes spatial gradients, recruitment rates to empty cells peak at midshore levels and high wave energies (fig. 2*A*). Along the vertical axis, recruitment rate declines from the peak midshore value to higher and lower shore levels according to a Gaussian-shaped curve. Along the horizontal axis, recruitment rate declines exponentially with decreasing wave energy. The gradient effects in recruitment are summarized by the function

$$\sigma_{xy} = \sigma_1 e^{-\gamma(1-x)} e^{-[(y-y_m)^2/2\nu]}, \quad (4)$$

where $\gamma = \ln(\sigma_1/\sigma_0)$, σ_0 and σ_1 are, respectively, minimum and maximum recruitment rates along the wave-energy gradient, y_m is the midshore level where recruitment rates reach a peak, and ν is a parameter that specifies the rate of recruitment decline with shore level moving away from the midtidal peak.

Mussel Growth

Mussels have indeterminate, environmentally influenced growth (Sebens 1987). Growth rates increase with longer immersion times (i.e., lower shore levels; Dehnel 1956; Garza 2005) and higher nutrient flux (i.e., higher wave energies; Leigh et al. 1987; Dahlhoff and Menge 1996). Growth proceeds asymptotically to maximum ("terminal")

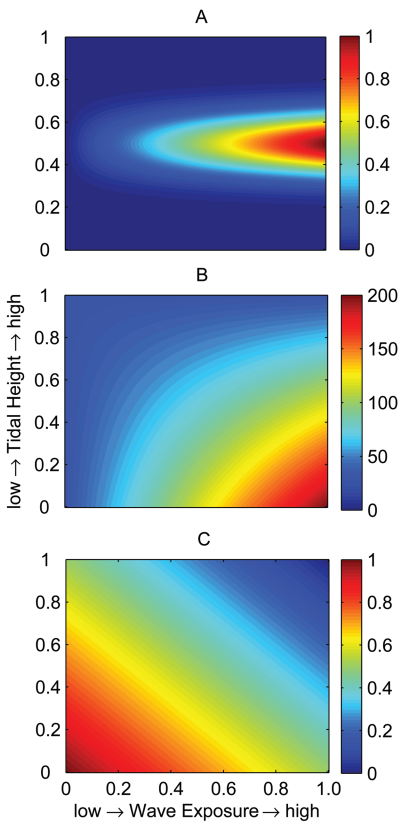

Figure 2: Landscape variation in recruitment rate σ (*A*), maximum size s_∞ (*B*), and predator attack rate θ (*C*).

sizes that vary along environmental gradients (Seed 1968, 1973; Kopp 1979; Robles et al. 2010). As in the ODE model, mussel growth follows the von Bertalanffy function,

$$\Delta S_{xy}(t) = \beta(s_{\infty,xy} - S_{xy}(t)). \tag{5}$$

The expected growth increment of a mussel, ΔS_{xy}, is proportional to the difference between the current size of a mussel, S_{xy}, and its maximum asymptotic size, $s_{\infty,xy}$, where β is the maximum growth rate. As in the empirical studies, the asymptotic size depends on flow rate and immersion time and therefore increases with increasing wave energy and decreasing shore level. For the spatial gradient in maximum size (fig. 2*B*), we use a simple product of linear trends along the horizontal and vertical dimensions,

$$s_{\infty,xy} = s_1 + (s_2 - s_1)x(1 - y), \tag{6}$$

where s_1 (30 mm) and s_2 (200 mm) are the minimum and maximum asymptotic sizes on the lattice and are based on field measurements (Robles et al. 2010).

Mussel Mortality, Predation, and Neighborhood Effects

The CA model includes two possible sources of mussel mortality: background mortality and predation. For simplicity, the same low rate of background mortality, μ_0, is assumed for all mussels independent of their size and location in the lattice. Background mortality includes all sources of mortality that are not explicitly from *Pisaster* predation, including physical stress and other predators. Experimental studies (Bertness and Grosholtz 1985; Fong 2009) indicate that younger, smaller mussels are shielded from predators by the larger, less vulnerable members of an aggregation. Thus, the CA model assumes that the likelihood of predation decreases as a mussel becomes surrounded by larger, less vulnerable individuals. Mortality rates due to predation are modeled as the product of predator density, $P(t)$, maximum per capita attack rate of predators at location (x, y), θ_{xy}, and the exponential decline in predation due to a size-dependent neighborhood effect. The total mortality rate of a mussel in cell (x, y) is given by

$$\mu_{xy}(t) = \mu_0 + \theta_{xy}P(t)e^{-c\bar{S}_{xy,r}(t)}, \tag{7}$$

where c is the resistance to predation due to increasing average mussel size in a neighborhood of radius r around (x, y), $\bar{S}_{xy,r}(t)$. Neighborhood mean mussel size density (including empty cells of size 0) is computed as a simple average of the size of the mussels in the grid of $(2r + 1) \times (2r + 1)$ cells centered at (x, y) in units of millimeters per cell,

$$\bar{S}_{xy,r}(t) = (2r + 1)^{-2} \sum_{i=x-r}^{x+r} \sum_{j=y-r}^{y+r} S_{ij}(t). \tag{8}$$

The maximum predation rate, θ_{xy}, varies with location on the lattice. Empirically, predation rates decrease with lengthening periods of tidal emersion (i.e., vertically toward higher shore levels; Paine 1974; Menge 1992; Robles et al. 1995; Garza 2005) and greater hydrodynamic stress (i.e., horizontally from sheltered to wave-exposed areas; Menge 1983; Sanford 2002). To model the gradient in maximum predator attack rate (fig. 2*C*), we use a simple linear trend from a high predation rate θ_1, at the lowest wave energy and lowest shore level, to a low rate θ_0, at the highest wave energy and highest shore level:

$$\theta_{xy} = \theta_0 + (\theta_1 - \theta_0)\frac{2 - x - y}{2}. \tag{9}$$

Mussel mortality in the CA model is equivalent to that in the ODE model when the neighborhood includes all cells on the lattice (i.e., neighborhood mean mussel size density equals global mean mussel size density) and when maxi-

mum predation rate, θ_{xy}, is constant across the lattice (i.e., $\theta_0 = \theta_1$ in eq. [9]).

Predator Dynamics

Experimental evidence shows that sea stars aggregate when there are episodes of massive recruitment of small mussels and disperse when these preferred prey are reduced in abundance relative to the larger mussels (Robles et al. 1995). These sea star aggregations arise because individuals encountering masses of preferred (i.e., small) mussels suspend their usual vertical and alongshore foraging movements, thereby remaining in the concentration of preferred prey, until these prey are depleted, at which point the vertical and alongshore movements resume (Robles et al. 1995). Recent evidence indicates that *Pisaster* use tactile, rather than waterborne, chemical cues for foraging (R. Zimmer, personal communication), perhaps because waterborne cues are unlikely to give good directional information in high-water-motion environments. This makes aggregative movement toward preferred prey less likely; instead, we model predators with a constant immigration rate and an emigration rate that depends on foraging experience.

In our models, predator density is a global variable and is expressed as an immigration-emigration process. We assume that predators enter the system at a constant rate I and exit the system at a per capita rate $E_P(t)$ that is inversely proportional to the per capita rate of prey consumption,

$$E_P(t) = \frac{e_0}{(wh)^{-1}\sum_{x,y} S_{xy}(t)\theta_{xy}e^{-c\bar{S}_{xy,r(t)}}}, \tag{10}$$

where the sum in the denominator is the total size density of mussels lost to predation over all the cells in the lattice. The parameter e_0 is the constant of inverse proportionality between mussels consumed and the rate of emigration.

Stochastic Processes in the CA Model

In the CA model, mussel recruitment, growth, and mortality are treated as stochastic events. For mussel recruitment and mortality, this was done by choosing an iteration time step Δt (default value for $\Delta t = 4$ days) and assuming that rates are constant within that time step. This assumption yields an exponential function for the probabilities. The probability of a recruitment event into an empty cell (x, y) is given by

$$\Pr\{S_{xy}(t + \Delta t) = 1 | S_{xy}(t) = 0\} = 1 - e^{-\sigma_{xy}(t)\Delta t}. \tag{11}$$

Similarly, the probability that a mussel in cell (x, y) dies is given by

$$\Pr\{S_{xy}(t + \Delta t) = 0 | S_{xy}(t) > 0\} = 1 - e^{-\mu_{xy}(t)\Delta t}. \tag{12}$$

Each mussel that dies is assigned a cause of death: background mortality, with probability $\mu_0/\mu_{xy}(t)$, or predatory mortality, with probability $1 - \mu_0/\mu_{xy}(t)$. Mussels consumed by predators in each time step are tracked in variable $\hat{C}(t)$, which is used in the computation of predator emigration rates (see below). If a mussel escapes a random mortality event, then it may experience a growth event in that time step. While this assumed ordering of survival followed by growth seems arbitrary, from a practical consideration, growth occurs slowly on the timescale of our model iterations, so that this assumption is of little importance. We use a truncated Poisson distribution to model mussel growth between integer size classes i, which allows integer increments between time steps that are greater than 1. The probability that a size-i mussel will grow to be size $i + j$ during time increment Δt is defined as

$$\Pr\{S_{xy}(t + \Delta t) = i + j | S_{xy}(t) = i\} = \begin{cases} \dfrac{e^{-\lambda_{xy}}\lambda_{xy}^{j}}{j!} & 0 \le j < s_{\infty,xy} - i, \\ 1 - \displaystyle\sum_{k=0}^{s_{\infty,xy}-i-1} \dfrac{e^{-\lambda_{xy}}\lambda_{xy}^{k}}{k!} & j = s_{\infty,xy} - i, \\ 0 & j > s_{\infty,xy} - i, \end{cases} \tag{13}$$

where $\lambda_{xy} = \Delta S_{xy}\Delta t$ (from eq. [5]) is the expected growth increment over the time interval Δt.

Predator immigration and emigration are handled as a stochastic birth-death process. However, predator movements occur on a much faster timescale than do changes in mussel size, and these timescales must be handled appropriately in the simulations. For example, the expected number of predator immigrants is $whI\Delta t$, which may, in fact, exceed the theoretical equilibrium number of predators unless Δt is small. On the other hand, if Δt is too small, then the size density of prey eaten, $\hat{C}(t)$, may fluctuate near 0, causing the predator emigration rate to approach infinity and the probability of emigration to approach 1. Therefore, a second, shorter time step of $\Delta\tau = \Delta t/n$ was used for predator immigration and emigration events in the CA model. During the time interval Δt, mussel densities remain constant, while predators randomly enter and leave the system every $\Delta\tau$. On this fast timescale, the probability that j predators enter the system is given by a Poisson distribution,

$$\Pr\{\Lambda(t + \Delta\tau) = j\} = \frac{e^{-whI\Delta\tau}(whI\Delta\tau)^{j}}{j!}, \tag{14}$$

where $\Lambda(t + \Delta\tau)$ is the number of predators entering the system. For emigration, the probability that an individual predator leaves the system is calculated with equation (10),

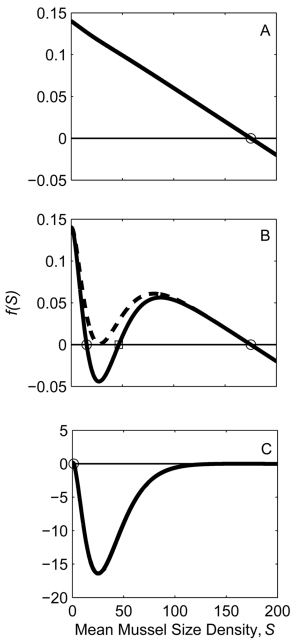

Figure 3: Plots of $f(S)$ versus S (eq. [2]) for three values of predator attack rate θ: *A*, the mean-field model exhibits a single stable upper equilibrium when $\theta = 0.1$; *B*, the solid line indicates stable upper ($S^* = 174$ mm cell^{-1}) and lower ($S^* = 14.5$ mm cell^{-1}) equilibria separated by an unstable equilibrium when $\theta = 1$; the dashed line indicates transition from a single equilibrium to multiple equilibria; *C*, a single stable lower equilibrium for $\theta = 10$. Stable equilibria are indicated by circles; unstable equilibria are indicated by squares. All other parameters are at the default values (table 1).

where the summation in the denominator is replaced with $\hat{C}(t)$, the actual summed sizes of mussels consumed by sea stars during the previous time interval Δt. The probability that a single predator emigrates during the time interval $\Delta\tau$ equals

$$e_{\mathrm{p}} = 1 - e^{-\Delta\tau e_0 whP(t)/\hat{C}(t)}, \tag{15}$$

and the probability that j predators emigrate is given by the binomial distribution

$$\Pr\{\Upsilon(t + \Delta\tau) = j\} = \binom{whP(t)}{j} e_{\mathrm{P}}^{j}(1 - e_{\mathrm{P}})^{whP(t)-j}, \tag{16}$$

where $\Upsilon(t + \Delta\tau)$ is the number of predators leaving the system and $whP(t)$ is the number of predators at the beginning of the time interval (product of the lattice size and the predator density). At the end of each time interval $\Delta\tau$, the new predator density equals

$$P(t + \Delta\tau) = P(t) + \frac{\Lambda(t + \Delta\tau) - \Upsilon(t + \Delta\tau)}{wh}. \tag{17}$$

Equation (17) is iterated n times for every Δt time step.

Results

Dynamics of the Mean-Field Model

The solution to the mean-field model gives rise to three cases: (1) a single stable equilibrium (attracting node) of high mean mussel size density (upper S^*; fig. 3*A*), (2) a single stable equilibrium (attracting node) of low mean mussel size density (lower S^*; fig. 3*C*), or (3) two stable equilibria (attracting nodes) of high (upper S^*) and low (lower S^*) mean mussel size density separated by an unstable equilibrium (saddle point; fig. 3*B*).

At the upper S^*, mussels are, on average, at a larger, more predator-resistant size, which corresponds to a low predator density equilibrium (lower P^*) because predator emigration is high when per capita mussel consumption is low (eq. [10]). The upper S^* is the only stable equilibrium (as in fig. 3*A*) when predator attack rate θ is low (fig. 4*A*), resistance to predation c is high (fig. 4*B*), mussel growth rate β is high (fig. 4*D*), or predator emigration

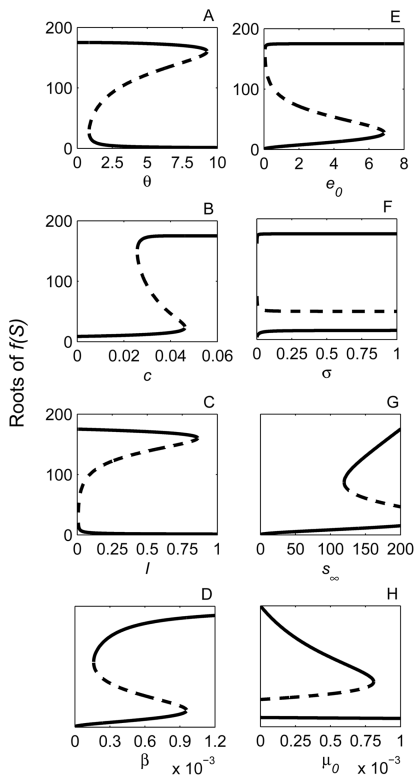

Figure 4: Bifurcation plots of equilibrium mean mussel size density (S^*, the roots of eq. [2]), for predator attack rate θ (*A*); predation resistance c (*B*); predator immigration I (*C*); mussel growth rate β (*D*); predator emigration constant e_0 (*E*); recruitment rate σ (*F*); maximum size, s_∞ (*G*); and background mortality rate μ_0 (*H*). Solid lines represent stable equilibria, and dashed lines represent unstable equilibria.

rate e_0 is high (fig. 4*E*). At the lower S^*, mussels are, on average, at a smaller, more vulnerable size, which corresponds to a high predator density equilibrium (upper P^*) because predator emigration is low when per capita mussel consumption by predators is high (eq. [10]). The lower S^* is the only stable equilibrium (as in fig. 3*C*) when predator attack rate θ is high (fig. 4*A*), resistance to predation c is low (fig. 4*B*), predator immigration I is high (fig. 4*C*), mussel growth rate β is low (fig. 4*D*), or background mortality rate μ_0 is high (fig. 4*H*). When the lower S^* is the only equilibrium (fig. 3*C*), mussels are consumed almost immediately after recruitment; practically, this is a no-mussel equilibrium.

For a range of parameter values, both upper and lower equilibria exist and are separated by an unstable equilibrium (fig. 4), and the system state depends on initial conditions (fig. 5*A*, 5*B*). This system is characterized by two alternative stable states and exhibits hysteresis: a small parameter change (e.g., a decrease in predator attack rate θ from 3 to 1; fig. 4*A*) can result in a dramatic shift in the state variable (mean mussel size density moves from the lower S^* to the upper S^*), but reversing that parameter change (increasing θ from 1 to 3) does not reverse the effect (mean mussel size density remains at the upper S^*). In this model, hysteresis results from size-dependent predation. Mussel beds with high mean size density are resistant to predation: predators immigrate into the system and find few mussels of preferred size to eat, resulting in a high emigration rate and low predation pressure. Mussel beds with low mean size density are susceptible to predation: predators immigrate into the system and find many mussels of preferred size, resulting in a low emigration rate and high predation pressure that prevents mussels from reaching more predator-resistant sizes. Both of these states have positive feedbacks, resulting in hysteresis.

Comparison of the Mean-Field and CA Models

When neighborhood size is equal to the entire arena (i.e., a "global" neighborhood) and the landscape is uniform, the CA model is a stochastic simulator of the ODE model (fig. 5). For the default parameter values (table 1), the system displays two stable equilibria separated by an unstable equilibrium (fig. 3*B*), and the system state depends on the initial conditions. When initial mean mussel size density is below the unstable equilibrium, the system converges to the lower equilibrium (lower S^*; blue and green lines in fig. 5), which is dominated by small mussels (fig.

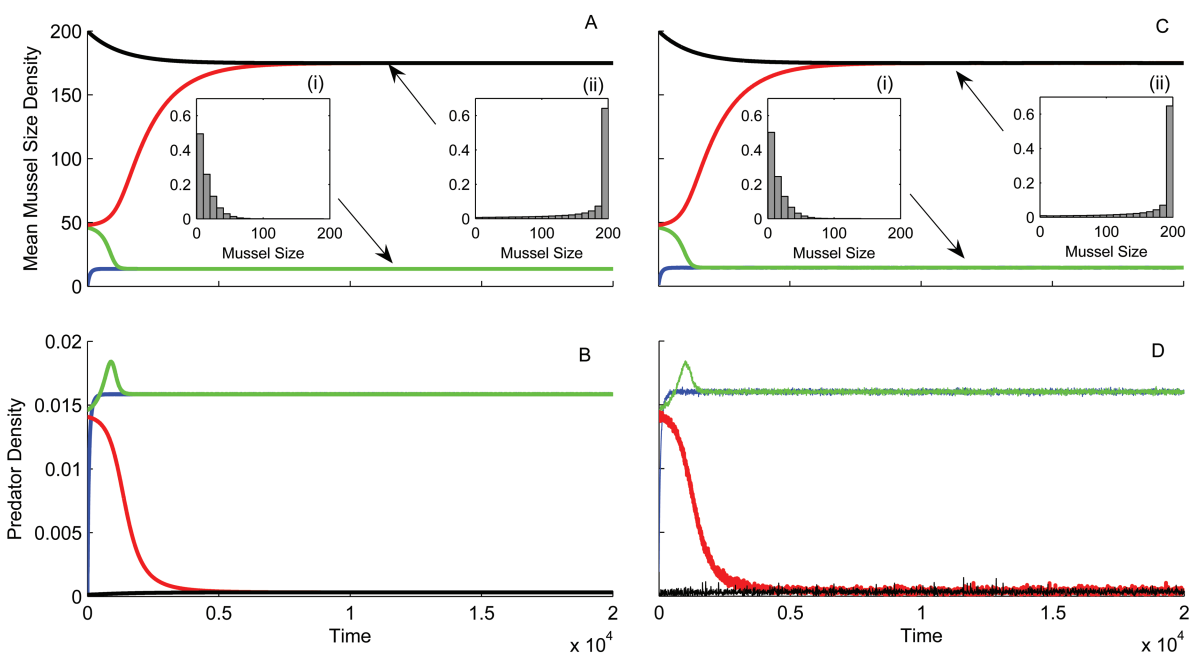

Figure 5: Comparing the ordinary differential equation (ODE) model (eq. [1]; *A*, *B*) with the cellular-automaton (CA) simulation (*C*, *D*) when the CA model is spatially homogeneous and has a global neighborhood. The upper panels display mean mussel size density through time in the ODE (*A*) and CA (*C*) models; insets display the size-frequency distribution of mussels at the lower (*i*) and upper (*ii*) equilibria. The lower panels display predator density through time in the ODE (*B*) and CA (*D*) models. Four initial conditions are plotted: $S(0) = 0$ (blue), 46 (green), 48 (red), and 200 (black).

5*Ai*, 5*Ci*) and has high predator density (fig. 5*B*, 5*D*, upper P^*). When initial mean mussel size density is above the unstable equilibrium, the system converges to the upper equilibrium (upper S^*; red and black lines in fig. 5), which is dominated by large mussels (fig. 5*Aii*, 5*Cii*) and has low predator density (fig. 5*B*, 5*D*; lower P^*). The CA model duplicates both transient and equilibrium behavior of the ODEs for mussel density, mussel size distribution, and predator density.

Effects of Spatially Local Interactions in Homogeneous Space

Spatially local interactions change the equilibrium dynamics (fig. 6). When predation risk depends on global mean mussel size density in the CA model, a mussel bed establishing on bare substrate ($S(0) = s_0$) remains at the lower equilibrium (fig. 6; dashed black line: r = global), as expected from the ODE model (fig. 5*A*). However, when predation risk depends on local mussel size density, a mussel bed establishing on bare substrate ($S(0) = s_0$) reaches the upper equilibrium (fig. 6, green line: $r = 0$; dashed blue line: $r = 1$). When $r = 0$ (fig. 6, green line), predation depends only on individual mussel size: individual mussels become resistant to predation, and the system reaches the upper equilibrium (fig. 6*i*). When $r = 1$ (fig. 6, dashed blue line), large mussels provide protection to neighboring mussels and patches of large, predator-resistant mussels form (fig. 6*ii*) and expand to establish the upper equilibrium (fig. 6*i*). When $r \geq 2$ (fig. 6, red line: $r = 2$, dashed black line: r = global), any size advantage gained by a mussel is diluted by the smaller size of its neighbors; as a result, predation risk is high and the system remains at the lower equilibrium (fig. 6*iii*). Therefore, when the environment is spatially homogeneous, very small neighborhoods ($r = 0, 1$) allow the system to reach the upper equilibrium; however, with even moderate-sized neighborhoods ($r \geq 2$), the system behaves as if well-mixed. Note that although per predator predation risk is local ($\theta_{xy} e^{-c\bar{S}_{xy}}$), overall predator density is influenced by all mussels in the arena through predator emigration rate (eq. [10]).

Boundary Formation along a One-Dimensional Environmental Gradient

Consider a one-dimensional, linear gradient in predator attack rate, $\theta = [3, 0]$, along the Y-axis (fig. 7*A*), which represents decreasing predation risk with increasing tidal height. In the ODE model, the equilibrium solution shifts from a single stable upper equilibrium in mean mussel size density to simultaneously stable upper and lower equi-

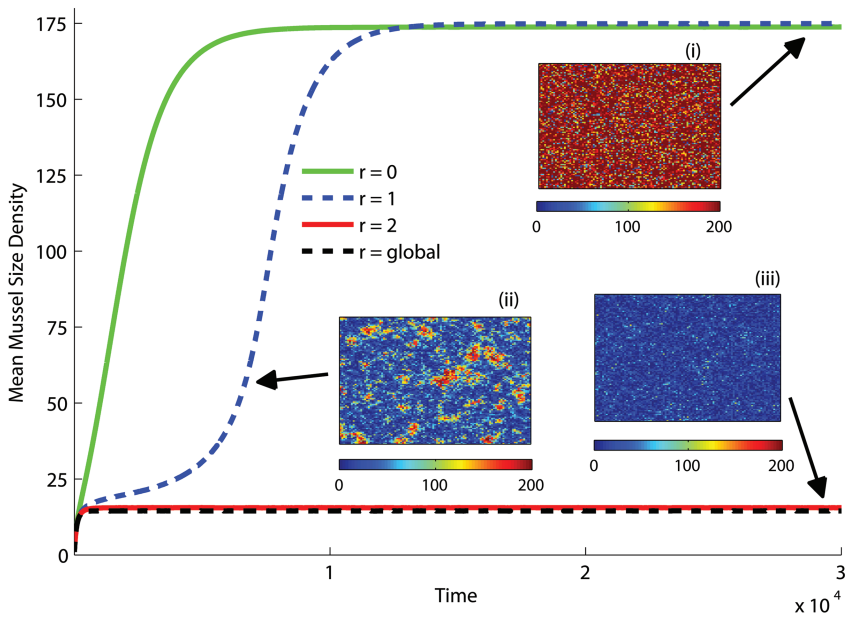

Figure 6: Neighborhood effects in homogeneous space: cellular-automaton model simulations for neighborhoods $r = 0$ (green line), 1 (dashed blue line), 2 (red line), and global (dashed black line). Insets illustrate the upper equilibrium (*i*; upper S^*, $r = 0$ at $t = 40{,}000$), the transition from lower to upper equilibrium (*ii*; $r = 1$ at $t = 6{,}000$), and the lower equilibrium (*iii*; lower S^*, $r = 2$ at $t = 40{,}000$). The color bars indicate mussel size S (mm).

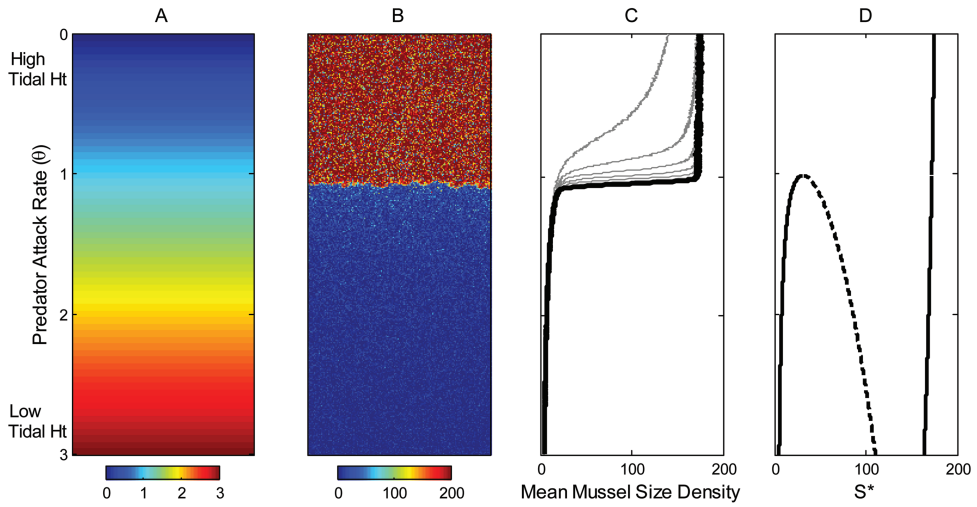

Figure 7: Concordance of mussel bed boundary in a cellular-automaton (CA) model and multiple equilibria in an ordinary differential equation (ODE) model along a gradient in predator attack rate (θ). *A*, One-dimensional landscape gradient in θ from a low-intertidal value of 3 to a high-intertidal value of 0; the color bar indicates the value of θ. *B*, Steady state of a CA mussel bed simulated on the landscape from *A* with a linear tidal gradient in θ when $r = 2$ ($t = 20 \times 10^3$); the color bar indicates mussel size (mm). *C*, Tidal height versus mussel size density in the CA model; lines show progression through time (every 3×10^3 time steps, thin gray lines) until a stable boundary is reached (thick black line). *D*, Stable (solid lines) and unstable (dashed line) equilibrium solutions of the ODE (S^*) for each level of θ at the steady state predator density ($P = 0.00131$ at $t = 20 \times 10^3$) in *B*.

libria when solved at values of $\theta = [0, 3]$ (fig. 4*A*). When a CA model with spatially local interactions ($r = 2$) is used, a sharp boundary in mussel size emerges on this linear gradient in attack rate (fig. 7*B*). Mussels in the high intertidal experience lower predation risk and grow to reach maximum size; the boundary forms higher in the intertidal and shifts downward through time until a stationary boundary location is achieved (fig. 7*C*). The location of the boundary corresponds to the shift from one to two stable equilibria in the ODE model (fig. 7*D*), when the ODE model is solved with the global predator density from the CA model arena.

In contrast to dynamics without gradients (fig. 6), boundary formation in the presence of an environmental gradient is robust to neighborhood size. For a wide range of intermediate neighborhood sizes ($1 \leq r \leq 25$; fig. C1, available online), a boundary forms along the gradient in predator attack rate that corresponds to the shift from one to two stable equilibria in the ODE model. The sharpness and precise location of this boundary depend on neighborhood size (fig. C1).

Effects of Varying Predator Immigration in the Presence of an Environmental Gradient

Global predator density links the predation risk of all mussels in the arena, while neighborhood effects link per predator predation risk at smaller scales. The existence of the mussel bed boundary depends on local interactions, while the location of the boundary depends on global predator density. To demonstrate the sensitivity of boundary location to predator density, we varied predator immigration rate (I), mimicking the removal (lower I) or addition (higher I) of *Pisaster* in field experiments (Robles et al. 2009). Halving predator immigration rate (i.e., removing *Pisaster* from a mussel bed) halved predator density and resulted in extension of the mussel bed lower into the intertidal. Doubling the predator immigration (i.e., adding *Pisaster* to a mussel bed) increased predator density by 50% and resulted in retraction of the mussel bed higher into the intertidal (fig. 8). The resulting *Pisaster* densities (0.5, 0.33, and 0.17 m^{-2} for addition, control, and removal, respectively) and mussel bed dynamics in the model are concordant with the results of recent field experiments manipulating *Pisaster* density and tracking mussel bed response (figs. 1, 3 in Robles et al. 2009).

Emergent Properties in the Spatial Structure of Mussel Beds

To investigate a field-relevant scenario (Robles et al. 2009, 2010), we examined a two-dimensional arena with the vertical and horizontal gradients representing the effects of tidal emergence and wave exposure, respectively, on

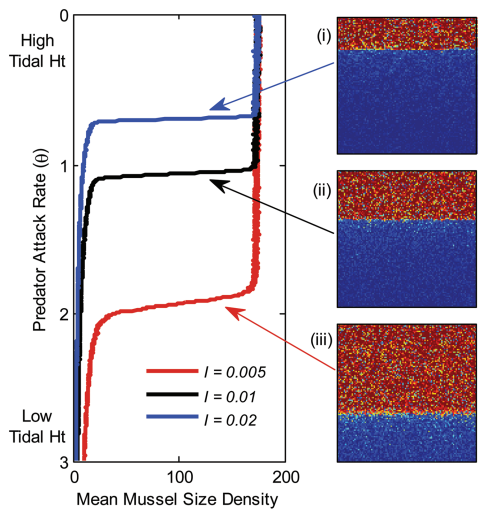

Figure 8: Mussel bed boundary location for three levels of predator immigration: *i*, $I = 0.02$ (blue line) is a doubling of the immigration rate that increases predator density by 50%, to $P = 0.020$ cell^{-1} (~0.5 m^{-2}); *ii*, $I = 0.01$ (black line) is the default immigration rate that results in a predator density of $P = 0.013$ cell^{-1} (~0.33 m^{-2}); and *iii*, $I = 0.005$ (red line) is a halving of the immigration rate that decreases predator density by 50%, to $P = 0.0067$ cell^{-1} (~0.17 m^{-2}). The main panel plots tidal height (and predator attack rate θ) versus the mean size density of mussels in the cellular-automaton model, and adjacent panels display the arena at three levels of immigration. All other parameters are at default values, and $r = 2$. All figures are plotted at $t = 20 \times 10^{-3}$ time steps.

recruitment (σ), maximum size (s_∞), and predator attack rate (θ), as illustrated in figure 2. Alongshore gradients of wave energy are ubiquitous in field systems where the swell impinges on windward rock surfaces and dissipates its force leeward. Realistic gradients in θ and s_∞ can, separately, result in transitions from single to multiple stable equilibria (fig. 4*A*, 4*G*), and both equilibria exist for all meaningful values of σ (fig. 4*F*). Combining gradients in all three parameters (fig. 2), we solved the ODE model for the parameter set (σ_{xy}, θ_{xy}, $s_{\infty, xy}$) at each location in the idealized two-dimensional landscape and identified regions with either a single stable equilibrium or two stable equilibria (fig. D1, available online). The simulated steady state is a wedge-shaped mussel bed (fig. 9*A*) that reflects patterns observed in the field (this comparison is detailed in Robles et al. 2010). At high wave exposures, the character and location of the lower mussel bed boundary is similar to that in the one-dimensional model: the boundary is abrupt and corresponds to the shift from one to two stable equilibria in the ODE model (fig. 9*Aii*, 9*Aiii*, 9*B*, 9*C*, D1). This shift from one to two stable equilibria occurs only at the five higher levels of wave exposure (note the unstable equilibria indicated by asterisks in fig. 9*C* for wave exposures ≥ 0.55). At lower wave exposures, only a single equilibrium exists and the lower edge of the simulated mussel bed is gradual (fig. 9*Ai*, 9*B*), corresponding to a phase shift in a single stable equilibrium (figs. 9*C*, D1). The upper mussel bed boundary is gradual for all wave exposures (fig. 9*B*), reflecting a phase shift in the single stable-equilibrium solution as a function of the underlying landscape gradients (figs. 9*C*, D1).

The lower boundaries of real mussel beds show the same alongshore trend in location and intensity, but to a lesser degree. Areas with reduced wave exposure have mussel bed boundaries that are less distinct and are at higher tidal heights than modeled boundaries (Robles et al. 2010). While neighborhood effects remain present in low-wave-energy regions, the maximum benefit afforded by the neighborhood declines as maximum mussel size declines; thus, the strength of the neighborhood effects diminishes, but is not lost, over the gradient.

Discussion

The classic verbal model for the sharp lower boundary of mussel beds posited a fixed spatial refuge from predators, suggesting that this dramatic ecological threshold reflects an equally dramatic underlying shift in predator attack rate. In contrast, the model presented here posits a dynamic equilibrium, in which this dramatic ecological threshold results from the switch from one to two stable equilibria along smooth environmental gradients. This conceptualization better captures empirical observations and experiments (Robles et al. 2009), including the crucial experiment demonstrating the retraction of the mussel bed with increased *Pisaster* density (fig. 8), contra expectations of the fixed-spatial-refuge theory.

The abrupt mussel bed boundary in the CA model corresponds to the transition from one to multiple equilibria in the ODE model (figs. 7*C*, 7*D*, D1) when the ODE is solved at each level of predator attack rate using the global predator density from the CA model. The alignment of the CA boundary and the ODE equilibria transition is noteworthy because the ODE predictions are mean-field solutions of mussel size density assuming constant predator density, while the CA model is a dynamic, two-scale system with global feedback through predator density and local feedback through mussel size density.

An important aspect of boundary formation in the one-dimensional CA model is the gradual downward expansion of the mussel bed through time (fig. 7*C*): starting in an empty arena, mussels grow to large size in low-predation-risk areas and then confer decreased predation risk to neighboring mussels, allowing expansion into riskier areas. In the CA model, this decreased risk arises in two ways: (1) locally, new recruits at the edge of the mussel bed have

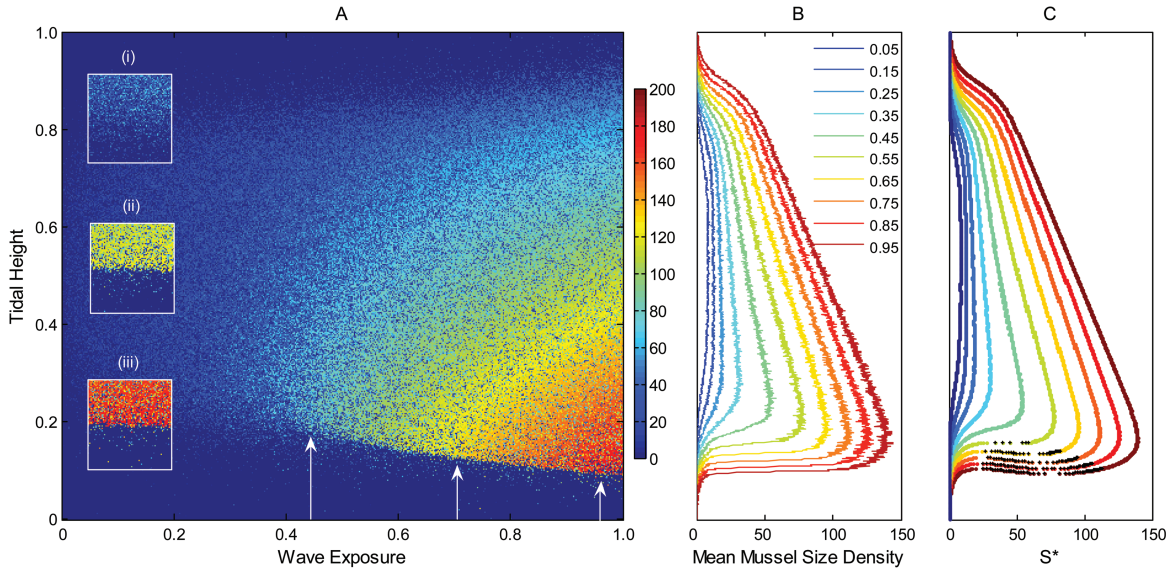

Figure 9: Mussel bed formation in a cellular-automaton (CA) model simulation and an ordinary differential equation (ODE) model varying in tidal height (*Y*-axis) and wave exposure (*X*-axis). *A*, Established mussel bed in the CA model with $r = 2$; the color bar indicates individual mussel size (mm). *B*, Mean mussel size density in the CA model at 10 levels of wave exposure, scaled from 0 to 1 (see key). *C*, ODE equilibrium solutions at parameter values corresponding to the same tidal heights and wave exposures as in *B* (see key in *B*), solved at the steady state predator density in *A*; unstable equilibria are plotted as black asterisks. The insets in *A* magnify the lower boundary at $x = 0.35$, (*i*), $x = 0.65$ (*ii*), and $x = 0.95$ (*iii*), indicated by white arrows.

decreased predation risk because of protection from large neighboring mussels, and (2) globally, as more of the arena is occupied by larger, less-preferred mussels, predator consumption declines and predator emigration rates increase, leading to lower global predator densities. As the ODE model is solved with declining predator densities from the CA model, the boundary between single and multiple equilibria shifts downward to higher predator attack rates (fig. 7*D*). This mussel bed expansion has dynamics similar to those of an invasion front with Allee effects (Keitt et al. 2001): the invasion expands when the benefits accrued from high-density neighboring cells within the front overcome the costs of low density in cells adjacent to the front, and the front stabilizes when the benefits accrued from high-density neighbors no longer outweigh the costs of the low-density neighbors (Keitt et al. 2001). This transition from expansion to stability is equivalent to the transition from single to multiple equilibria (dashed line to black line in fig. 3*B*; Keitt et al. 2001). In our model, the mussel bed boundary ultimately stabilizes where the buildup of large mussels on the boundary no longer outweighs the increased risk in adjacent cells.

The tendency for local interactions to change dynamics from the mean-field predictions depends on the landscape. On a homogeneous landscape (fig. 6), equilibrium behavior is highly sensitive to the scale of neighborhood effects: only the smallest neighborhoods ($r = 0, 1$) deviate from well-mixed behavior by converging on the upper equilibrium. On more realistic heterogeneous landscapes (here, a one- or two-dimensional gradient), boundary formation is robust to a wide range of neighborhood sizes (fig. C1), even though the well-mixed model remains at the lower equilibrium (fig. C1*A*; $r =$ global). The difference between the ODE predictions based on the CA model predator density (fig. 7*D*) and the full equilibrium solution of equation (3) (fig. 4*A*) demonstrates the importance of local interactions. In both the homogeneous and the heterogeneous landscapes, local interactions allow mussels to occupy a larger proportion of the entire arena. The scale of local interactions also influences the character of the lower boundary (fig. C1*C*–C1*G*). However, subtle changes in boundary character with neighborhood size may be less important than larger changes over the boundary range (see fig. 9 and discussion below) and less important in the field because of small-scale heterogeneities in the physical features in the intertidal. More important is that boundary formation is robust over a wide range of neighborhood sizes. Future work should consider the effects of small-scale landscape heterogeneities on mussel bed structure

and boundary formation when those heterogeneities are at a scale similar to that of local interactions.

The full two-dimensional simulation (fig. 9) demonstrates several patterns that are concordant with field observations, including boundary location and fragmentation (Robles et al. 2009, 2010). In this dynamical system, we find both abrupt and continuous boundaries, where the abrupt boundaries correspond to bifurcations from one to multiple equilibria (figs. 7, 9*C*, D1) and the continuous boundaries correspond to phase shifts in a single equilibrium. Previous studies on species range limits (Holt and Keitt 2000; Keitt et al. 2001; Holt et al. 2005) have noted how Allee effects can result in sharp species boundaries, in contrast to more gradual species boundaries that result from changes in colonization and extinction rates. This model posits this same variation in the nature of species boundaries over a much smaller spatial scale. We conceived this model at the scale of an intertidal mussel bed (tens of meters); in this system, the neighborhood effects (decreased predation with increased mussel size) vary in magnitude over a few meters and result in distinct boundary types within the same dynamical system. In areas of the landscape with large maximum mussel size and moderate predator attack rate (lower right in the two-dimensional gradients; fig. 2), neighborhood effects result in multiple equilibria (figs. 9*C*, D1*B*) and therefore sharp boundaries (fig. 9*A*). In other parts of the landscape, the same underlying model sharing the same predator population results in a single equilibrium (figs. 9*C*, D1*A*), which has continuous boundaries corresponding to the slow change of underlying parameter values (fig. 9*A*). This model provides an example, with corresponding empirical data (Robles et al. 2009, 2010), in which the same underlying model gives rise to species boundaries of different characteristics because of fundamentally different threshold dynamics in different regions of the landscape.

Like other models that generate spatial ecological thresholds from bifurcating equilibria (e.g., Wilson and Nisbet 1997; van de Koppel et al. 2005; Zeng and Malanson 2006), this model relies on locally positive and globally negative feedback. Wilson and Nisbet (1997) considered this problem directly in a general cell-occupancy model of intraspecific cooperation and competition and demonstrated that positive local interactions can generate a spatial threshold on a continuous gradient. The model presented here advances their work by connecting the theory to an explicit empirical system; in doing so, we demonstrate that boundary formation is robust to the additional complications of size-structured predator-prey interactions over a range of neighborhood sizes. More generally, the model presented here is an example of "classical criticality" as defined by Pascual and Guichard (2005), in which disturbance (predation on mussels) is well mixed and disturbance intensity depends on the local density of susceptible individuals. A characteristic of classical criticality is the presence of a threshold along a gradient of disturbance, as demonstrated here by the abrupt boundary between upper and lower mussel bed equilibria.

Combined with previous papers (Robles and Desharnais 2002; Robles et al. 2009, 2010), this work indicates a concordance between a dynamic predator-prey model and field experiments and observations, providing a new paradigm for understanding mussel bed boundaries. This concordance of field observation and model predictions at small spatial scales is based on empirical patterns of covariance between mussel growth rates, predator attack rates, and settlement patterns within mussel beds, as represented in figure 2. On regional spatial scales, however, these parameters may covary in different ways (Menge et al. 1994, 2004). Future work should focus on expanding predictions of this model to regional-scale patterns of boundary formation and location in the intertidal.

Acknowledgments

This work was improved by discussions with C. Garza, F. Guichard, R. Nisbet, and J. van de Koppel. The work was supported by National Science Foundation grants HRD-0317772, OCE 0089842, and EF-0827595.

Literature Cited

Bertness, M. D., and E. Grosholz. 1985. Population dynamics of the ribbed mussel, *Geukensia demissa*: the costs and benefits of an aggregated distribution. Oecologia (Berlin) 67:192–204.

Connell, J. H. 1972. Community interactions on marine rocky intertidal shores. Annual Review of Ecology and Systematics. 3:169–192.

Dahlhoff, E. P., and B. A. Menge. 1996. Influence of phytoplankton concentration and wave exposure on the ecophysiology of *Mytilus californianus*. Marine Ecology Progress Series 144:97–107.

Dehnel, P. A. 1956. Growth rates in latitudinally and vertically separated populations of *Mytilus californianus*. Biological Bulletin 110: 43–53.

Denny, M. W. 1988. Biology and the mechanics of the wave-swept environment. Princeton University Press, Princeton, NJ.

Denny, M. W., and M. F. Shibata. 1989. Consequences of surf-zone turbulence for settlement and external fertilization. American Naturalist 134:859–889.

Donalson, D. D., R. A. Desharnais, C. D. Robles, and R. M. Nisbet. 2004. Spatial dynamics of a benthic community: applying multiple models to a single system. Pages 429–444 *in* L. Seuront and P. G. Strutton, eds. Handbook of scaling methods in aquatic ecology: measurement, analysis, simulation. CRC, Boca Raton, FL.

Dudgeon, S., R. Aronson, J. Bruno, and W. Precht. 2010. Phase shifts and stable states on coral reefs. Marine Ecology Progress Series 413:201–216.

Fong, L. S. 2009. Facultative interactions in populations of *Mytilus*

californianus in British Columbia, Canada. MS thesis. California State University at Los Angeles.

Garza, C. 2005. Prey productivity effects on the impact of predators of the mussel, *Mytilus californianus* (Conrad). Journal of Experimental Marine Biology and Ecology 324:76–88.

Groffman, P. M., J. S. Baron, T. Blett, A. J. Gold, I. Goodman, L. H. Gunderson, B. M. Levinson, et al. 2006. Ecological thresholds: the key to successful environmental management or an important concept with no practical application? Ecosystems 9:1–13.

Guichard, F., P. M. Halpin, G. W. Allison, J. Lubchenco, and B. A. Menge. 2003. Mussel disturbance dynamics: signatures of oceanographic forcing from local interactions. American Naturalist 161: 889–904.

Holt, R. D., and T. H. Keitt. 2000. Alternative causes for range limits: a metapopulation perspective. Ecology Letters 3:41–47.

Holt, R. D., T. H. Keitt, M. A. Lewis, B. A. Maurer, and M. L. Taper. 2005. Theoretical models of species' borders: single species approaches. Oikos 108:18–27.

Huggett, A. J. 2005. The concept and utility of "ecological thresholds" in biodiversity conservation. Biological Conservation 124:301–310.

Keitt, T. H., M. A. Lewis, and R. D. Holt. 2001. Allee effects, invasion pinning, and species' borders. American Naturalist 157:203–216.

Kopp, J. C. 1979. Growth and the intertidal gradient in the sea mussel *Mytilus californianus* Conrad, 1837. Veliger 22:51–56.

Lauzon-Guay, J. S., and R. E. Scheibling. 2010. Spatial dynamics, ecological thresholds and phase shifts: modeling grazing aggregation and gap formation in mussel beds. Marine Ecology Progress Series 403:29–41.

Leigh, E. G., R. T. Paine, J. F. Quinn, and T. H. Suchanek. 1987. Wave energy and intertidal productivity. Proceedings of the National Academy of Sciences of the USA 84:1314–1318.

May, R. M. 1977. Thresholds and breakpoints in ecosystems with a multiplicity of stable states. Nature 269:471–477.

Menge, B. A. 1983. Components of predation intensity in the low zone of the New England rocky intertidal region. Oecologia (Berlin) 58:141–155.

———. 1992. Community regulation: under what conditions are bottom-up factors important on rocky shores? Ecology 73:755–765.

Menge, B. A., E. L. Berlow, C. A. Blanchette, S. A. Navarrete, and S. B. Yamada. 1994. The keystone species concept: variation in interaction strength in a rocky intertidal habitat. Ecological Monographs 64:249–286.

Menge, B. A., C. Blanchette, P. Raimondi, T. Freidenburg, S. Gaines, J. Lubchenco, D. Lohse, G. Hudson, M. Foley, and J. Pamplin. 2004. Species interaction strength: testing model predictions along an upwelling gradient. Ecological Monographs 74:663–684.

Moya, P. C. 2005. Tests of three hypotheses and differential settlement in *Mytilus californianus* and *Mytilus galloprovincialis*. MS thesis. California State University at Los Angeles.

Mumby, P. J. 2009. Phase shifts and the stability of macroalgal communities on Caribbean coral reefs. Coral Reefs 28:761–773.

Muradian, R. 2001. Ecological thresholds: a survey. Ecological Economics 38:7–24.

Nisbet, R. M., S. Diehl, W. G. Wilson, S. D. Cooper, D. D. Donalson, and K. Kratz. 1997. Primary-productivity gradients and short-term population dynamics in open systems. Ecological Monographs 67: 535–553.

Osman, R. W., P. Munguia, and R. N. Zajac. 2010. Ecological thresholds in marine communities: theory, experiments and management. Marine Ecology Progress Series 413:185–187.

Paine, R. T. 1966. Food web complexity and species diversity. American Naturalist 100:65–75.

———. 1974. Intertidal community structure. Oecologia (Berlin) 15:93–120.

———. 1976. Size-limited predation: an observational and experimental approach with the *Mytilus-Pisaster* interaction. Ecology 57: 858–873.

Paine, R. T., and S. A. Levin. 1981. Intertidal landscapes: disturbance and the dynamics of pattern. Ecological Monographs 51:145–178.

Pascual, M., and F. Guichard. 2005. Criticality and disturbance in spatial ecological systems. Trends in Ecology & Evolution 20:88–95.

Petraitis, P. S., and S. R. Dudgeon. 2004. Detection of alternative stable states in marine communities. Journal of Experimental Marine Biology and Ecology 300:343–371.

Petraitis, P. S., and C. Hoffman. 2010. Multiple stable states and relationship between thresholds in processes and states. Marine Ecology Progress Series 413:189–200.

Robles, C., and R. Desharnais. 2002. History and current development of a paradigm of predation in rocky intertidal communities. Ecology 83:1521–1536.

Robles, C., R. Sherwood-Stephens, and M. Alvarado. 1995. Responses of a key intertidal predator to varying recruitment of its prey. Ecology 76:565–579.

Robles, C. D. 1997. Changing recruitment in constant species assemblages: implications for predation theory in intertidal communities. Ecology 78:1400–1414.

Robles, C. D., R. Desharnais, C. Garza, M. J. Donahue, and C. A. Martinez. 2009. Complex equilibria in the maintenance of boundaries: experiments with mussel beds. Ecology 90:985–995.

Robles, C. D., C. Garza, R. Desharnais, and M. J. Donahue. 2010. Landscape patterns in boundary intensity: a case study of mussel beds. Landscape Ecology 25:745–759.

Sanford, E. 2002. Water temperature, predation, and the neglected role of physiological rate effects in rocky intertidal communities. Integrative and Comparative Biology 42:881–891.

Scheffer, M., S. Carpenter, J. A. Foley, C. Folke, and B. Walker. 2001. Catastrophic shifts in ecosystems. Nature 413:591–596.

Sebens, K. P. 1987. The ecology of indeterminate growth in animals. Annual Review of Ecology and Systematics 18:371–407.

Seed, R. 1968. Factors influencing shell shape in the mussel *Mytilus edulis*. Journal of the Marine Biological Association of the United Kingdom 48:561–584.

———. 1973. Absolute and allometric growth in the mussel, *Mytilus edulis* L. (Mollusca: Bivalvia). Journal of Molluscan Studies 40: 343–357.

van de Koppel, J., and M. Rietkerk. 2004. Spatial interactions and resilience in arid ecosystems. American Naturalist 163:113–121.

van de Koppel, J., M. Rietkerk, N. Dankers, and P. M. J. Herman. 2005. Scale-dependent feedback and regular spatial patterns in young mussel beds. American Naturalist 165:E66–E77.

Wilson, W. G., and R. M. Nisbet. 1997. Cooperation and competition along smooth environmental gradients. Ecology 78:2004–2017.

Wootton, J. T. 2001. Local interactions predict large-scale pattern in empirically derived cellular automata. Nature 413:841–844.

Zeng, Y., and G. P. Malanson. 2006. Endogenous fractal dynamics at alpine treeline ecotones. Geographical Analysis 38:271–287.

Associate Editor: Marc Mangel
Editor: Ruth G. Shaw